Redox Biology 13 (2017) 508–521

Contents lists available at ScienceDirect

Redox Biology

journal homepage: www.elsevier.com/locate/redox

Research paper

Caveolin 1-related autophagy initiated by aldosterone-induced oxidation promotes liver sinusoidal endothelial cells defenestration

Xiaoying Luo[a,f,1], Dan Wang[a,1], Xuan Luo[b], Xintao Zhu[c], Guozhen Wang[a], Zuowei Ning[a], Yang Li[a], Xiaoxin Ma[a], Renqiang Yang[d], Siyi Jin[a], Yun Huang[a], Ying Meng[e,*], Xu Li[a,f,**]

[a] Guangdong Provincial Key Laboratory of Gastroenterology, Department of Gastroenterology, Nanfang Hospital, Southern Medical University, Guangzhou, China
[b] Department of Hepatobiliary Surgery, Guizhou Provincial People's Hospital, No. 52 Zhongshan East Road Nanming District, Guiyang, Guizhou Province, China
[c] Southern Medical University, Guangzhou, China
[d] Department of Emergency and Critical Care Medicine, Guangdong General Hospital & Guangdong Academy of Medical Sciences, Guangzhou, China
[e] Department of Respiratory Diseases, Nanfang Hospital, Southern Medical University, Guangzhou, China
[f] State Key Laboratory of Organ Failure Research, Guangdong Provincial Key Laboratory of Viral Hepatitis Research, Department of Infectious Diseases, Nanfang Hospital, Southern Medical University, Guangzhou, China

ARTICLE INFO

Keywords:
Autophagy
Liver sinusoidal endothelial cell
Defenestration
Aldosterone
Caveolin 1
Oxidation

ABSTRACT

Aldosterone, with pro-oxidation and pro-autophagy capabilities, plays a key role in liver fibrosis. However, the mechanisms underlying aldosterone-promoted liver sinusoidal endothelial cells (LSECs) defenestration remain unknown. Caveolin 1 (Cav1) displays close links with autophagy and fenestration. Hence, we aim to investigate the role of Cav1-related autophagy in LSECs defenestration. We found the increase of aldosterone/MR (mineralocorticoid receptor) level, oxidation, autophagy, and defenestration in LSECs in the human fibrotic liver, BDL or hyperaldosteronism models; while antagonizing aldosterone or inhibiting autophagy relieved LSECs defenestration in BDL-induced fibrosis or hyperaldosteronism models. *In vitro*, fenestrae of primary LSECs gradually shrank, along with the down-regulation of the NO-dependent pathway and the augment of the AMPK-dependent autophagy; these effects were aggravated by rapamycin (an autophagy activator) or aldosterone treatment. Additionally, aldosterone increased oxidation mediated by Cav1, reduced ATP generation, and subsequently induced the AMPK-dependent autophagy, leading to the down-regulation of the NO-dependent pathway and LSECs defenestration. These effects were reversed by MR antagonist spironolactone, antioxidants or autophagy inhibitors. Besides, aldosterone enhanced the co-immunoprecipitation of Cav1 with p62 and ubiquitin, and induced Cav1 co-immunofluorescence staining with LC3, ubiquitin, and F-actin in the perinuclear area of LSECs. Furthermore, aldosterone treatment increased the membrane protein level of Cav1, whereas decrease the cytoplasmic protein level of Cav1, indicating that aldosterone induced Cav1-related selective autophagy and F-actin remodeling to promote defenestration. Consequently, Cav1-related selective autophagy initiated by aldosterone-induced oxidation promotes LSECs defenestration via activating the AMPK-ULK1 pathway and inhibiting the NO-dependent pathway.

1. Introduction

Autophagy, a constitutive process that mediates encapsulation of damaged proteins, lipids or organelles in double-membrane autophagosomes for degradation, contributes to the maintenance of cellular homeostasis [1]. As a result, moderate autophagy facilitates cellular

Abbreviations: 3MA, 3-methyladenine; AMPK, AMP-activated protein kinase; ATP, adenosine triphosphate; ATP1B2, ATPase Na+/K+ transporting subunit beta 2; BDL, bile duct ligation; Cav1, Caveolin 1; CD31, platelet endothelial cell adhesion molecule-1, PECAM-1; cGMP, cyclic guanosine monophosphate; eNOS, endothelial nitric oxide synthase; LC3, microtubule-associated protein 1 light chain 3; LSEC, liver sinusoidal endothelial cell; MR, mineralocorticoid receptor; NAC, N-acetyl-L-cysteine; NO, nitric oxide; PKG, protein kinase G; ROS, reactive oxygen species; SEM, scanning electron microscopy; sGC, soluble guanylatecyclase; TEMPO, 2,2,6,6-tetramethylpiperidinooxy; mito-TEMPO, mitochondria 2,2,6,6-tetramethylpiperidinooxy; TEM, transmission electron microscopy; ULK1, unc-51 like autophagy activating kinase 1; VASP, vasodilator-stimulated phosphoprotein; vWF, von Willebrand Factor

* Correspondence to: Department of Respiratory Diseases, Nanfang Hospital, Southern Medical University, Guangzhou, China 510515.
** Correspondence to: State Key Laboratory of Organ Failure Research, Guangdong Provincial Key Laboratory of Viral Hepatitis Research, Department of Infectious Diseases, Nanfang Hospital, Southern Medical University, Guangzhou, 510515, China.
E-mail addresses: 519343749@qq.com (Y. Meng), mylx99@163.com (X. Li).
[1] These authors contributed equally to this work.

http://dx.doi.org/10.1016/j.redox.2017.07.011
Received 14 April 2017; Received in revised form 12 June 2017; Accepted 12 July 2017
Available online 13 July 2017

recycling and survival against extra-cellular detrimental stimuli, such as low nutrients, low ATP, and reactive oxygen species (ROS) [2]. Autophagy plays an essential role in the regulation of intra-hepatic cell function and metabolism. Autophagy attenuates the abnormal protein aggregates and protects hepatocytes against injury [3]. However, for hepatic stellate cells (HSCs), autophagy degrades triglyceride to activate HSCs [4].

In pathological conditions, liver sinusoidal endothelial cells (LSECs) display defenestration and capillarization, which initiates liver fibrosis. Recently, autophagy is reported to modulate the phenotype of LSECs and protect against acute liver injury induced by ischemia/reperfusion (I/R) [5]. However, how autophagy impacts on LSECs defenestration and capillarization, the preliminary step necessary for fibrogenesis and portal hypertension, is still unknown.

Aldosterone, the effector of the renin-angiotensin-aldosterone system (RAAS), has been evidenced to play a key role in organ fibrosis, such as in heart, renal, and liver tissue, via its pro-oxidative capacity [6,7]. Interestingly, aldosterone induced podocyte autophagy via oxidation [8], and the ROS-induced autophagy feed-back opposed aldosterone-induced podocyte injury by attenuating endoplasmic reticulum stress [9]. Given the pro-oxidation and pro-autophagy capabilities of aldosterone, in the present study, we focus on the effects of aldosterone on defenestration of LSECs and capillarization via initiation of oxidation and autophagy, which precedes the activation of HSCs and liver fibrogenesis. The mechanism of aldosterone in this process remains unclear.

Caveolin 1 (Cav1), a scaffolding/regulatory protein of caveolae on the plasma membrane of caveolae and on vesicles, displays close links with oxidation and autophagy. As a lipid raft molecule of caveolae in the membrane, Cav1 interacts with mineralocorticoid receptors (MR) and forms an MR/Cav1 complex in caveolae, which mediates a rapid signaling cascade of oxidation initiated by aldosterone [10]. The Cav1-mediated NADPH oxidase (NOX) promoted autophagy of intestinal epithelial cells [11]. In addition, Cav1 could interact with ATG12-ATG5 system to suppress autophagy in lung epithelial cells [12].

Moreover, being part of the cytoskeleton around fenestrae, F-actin modulates contraction of fenestrae [13], whose remodeling may facilitate defenestration. Autophagosome maturation was promoted by F-actin remodeling, and then, in turn, assembled an F-actin network and facilitated remodeling [14], indicating that autophagy contributes to F-actin remodeling and subsequent fenestrae contraction.

Consequently, Cav1 may be a multifunctional signaling hub that allows it to regulate aldosterone-induced oxidation, autophagy, and LSECs defenestration. Hence, the present study aims to investigate the role of Cav1-related autophagy in LSECs defenestration. We demonstrated for the first time that Cav1-related autophagy initiated by aldosterone-induced oxidation promotes LSECs defenestration.

2. Materials and methods

2.1. Reagents and antibodies

The reagents used included aldosterone (Sigma-Aldrich A9477, 52391), spironolactone (Sigma-Aldrich, S4054), 3MA (Sigma-Aldrich, S2767), rapamycin (Sigma-Aldrich, S1039), bafilomycin A1 (Sigma-Aldrich, SML1661), N-acetyl-L-cysteine (NAC, Sigma-Aldrich, A9165), TEMPO (Sigma-Aldrich, 426369), mito-TEMPO (Sigma-Aldrich, SML0737).

The antibodies used included anti-α-SMA (Boster, BM0002), anti-vWF (Santa Cruz, SC-365712), anti-vWF (Abcam, ab174290), anti-CD31 (Santa Cruz, SC-46694), anti-Cav1 (Abcam, ab17052), anti-Cav1 (Abcam, ab2910), anti-MR (Abcam, ab2774), anti-LC3 (Abcam, ab48394), anti-CD32b (Abclonal, A7554), anti-ubiquitin (Abcam, ab19247), anti-NOX4 (Abcam, ab60940), anti-p62 (Abcam, ab155686), anti-VASP (CST, 3132S), anti-eNOS (Abclonal, A1548), anti-AMPK (Proteintech, 10929-2-AP), anti-p-AMPK(Thr172) (Abclonal, AP0116), anti-ULK1 (Proteintech, 20986-1-AP), anti-p-ULK1(Ser555) (CST, S555), anti-ATP1B2 (Proteintech, 22338-1-AP), anti-GAPDH (Proteintech, 60004-1), and anti-β-actin (Proteintech, 60008-1). DAPI (Sigma-Aldrich, D9542), FITC-labeled goat anti-rabbit IgG (H + L) (Beyotime, a0562), and Cy3-labeled goat anti-mouse IgG (H + L) (Beyotime, a0521) were also used.

2.2. Patients

Fibrotic liver biopsy specimens (fibrosis stage: F3-4) were obtained from 9 patients with liver fibrosis due to bile duct stones (9 cases). Normal liver specimens were obtained from 6 patients who underwent a partial liver resection for hepatic hemangioma. All patients signed the informed written consent, and the Ethics Committee at the local hospital approved the use of samples.

2.2.1. Animal experimental design

Sprague-Dawley (SD) rats and C57 mice were provided by the Laboratory Animal Center (Southern Medical University, China) and were approved by the Committee on the Ethics of Animal Experiments of Southern Medical University. Animals were housed under a 12:12 h light/dark cycle at 22–24 °C.

2.2.2. BDL-induced liver fibrosis rat model

Male SD rats (180–220 g) were subjected to BDL (n = 72) or a sham operation (n = 16) for 28 days. At Days 3, 6, 9, 12, 15, 18, 21, 24, and 28, BDL-induced rats were randomly sacrificed (n = 4 per group). Alternatively, BDL-induced rats were randomly divided into a BDL group (n = 12 for 18 days and 28 days) and two therapy groups: co-treatment with spironolactone (40 mg/kg•d, gavage, n = 12 for 18 days and 28 days), 3MA (10 mg/kg•d, intraperitoneal injection, n = 12 for 18 days and 28 days).

2.2.3. Hyperaldosteronism (Aldosterone-Salt) model

In total, 36 male C57 mice (18–22 g) were randomly divided into five groups (vehicle-control, Aldosterone-Salt, and administration with spironolactone or 3MA; n = 9 per group). All mice were fed with 1% NaCl for 28 days. The Aldosterone-Salt and the two treatment groups were treated with aldosterone (0.1 μg/g h) continuously via osmotic mini-pumps for 28 days, while the two therapy groups were co-treated with spironolactone (40 μg/g d, gavage), 3MA (15 μg/g d, intraperitoneal injection).

2.3. Measurement of serum aldosterone

The serum aldosterone was detected by an aldosterone ELISA Kit (Elabscience, E-EL-0070c), according to the manufacturer instructions. The results were read and calculated by ELIASA.

2.4. Histological analysis and immunohistochemistry

Paraffin sections (4 μm) of animal and human liver tissues were prepared with hematoxylin and eosin (H & E) staining and Sirius Red staining. Immunohistochemical detection of α-SMA and vWF, were performed on paraffin sections (4 μm), and subsequent sections were exposed to HRP-antibody colored with DAB, and visualized by microscopy (BX51, Olympus, Japan). The degree of liver fibrosis and the number of α-SMA- or vWF-positive cells were quantified with Image J software.

2.5. Fluorescence staining

Paraffin sections (4 μm) were prepared for immunofluorescence, incubated with primary antibody overnight, followed by the secondary antibody, and then mounted with DAPI. The primary antibodies included anti-CD31 (1:200), anti-vWF (1:50), anti-MR (1:200), and anti-

LC3 (1:200). The secondary antibodies included FITC-labeled goat anti-rabbit IgG (H + L) (1:200) and Cy3-labeled goat anti-mouse IgG (H + L) (1:200).

2.6. SEM and TEM

The primary LSECs and liver tissues were fixed with 2.5% glutaldehyde and subsequently dehydrated and then coated with gold using the coating apparatus. Eventually, the LSECs fenestrae of samples were observed with SEM at 15-kV acceleration voltage. Additionally, the samples for TEM were stained with uranyl acetate and lead citrate, and autophagosomes and autolysosomes were observed using TEM at an 80-kV acceleration voltage.

2.7. Cell isolation, identification, culture and treatment

Primary rat LSECs were isolated from male SD rats, based on the modified method [15]. The isolated LSECs were identified by an SEM test and expression of CD31 and CD32b protein, which was detected by flow cytometry and confocal microscopy. LSECs were cultured in plates with medium comprising 40% MCDB131 (Gibco, 10372019), 40% 1640 (Gibco, 11875101) and 20% fetal bovine serum (FBS, TransSerum, 10102). Primary LSECs were stimulated by aldosterone with a concentration gradient of 0, 1, 10, 100 nM for 3 days and pretreated with spironolactone (20 μM), rapamycin (10 nM), 3MA (10 μM), bafilomycin A1 (10 nM), NAC (1 mM), TEMPO (1 μM), mito-TEMPO (100 U/ml).

2.8. Monitoring LSECs autophagic flux

Primary rat LSECs were transfected with an mRFP-GFP-LC3 encoding plasmid (Hanbio, LP2100001). Transfection efficiency was 70%. To detect autophagy flux in LSECs, the above treatments were used, and autophagic flux was visualized with confocal microscopy (Fluoview FV10i, Olympus, Japan).

2.9. Immunocytochemistry

Paraformaldehyde-fixed primary cells were incubated with the primary antibody, followed by the secondary antibody, and subsequently mounted with DAPI. The primary antibodies included anti-Cav1 (1:50), anti-LC3 (1:200), and anti-ubiquitin (1:100). To detect F-actin, after incubation with primary antibody and the secondary antibody, cells were stained with phallotoxins (Thermo, F432). The number of puncta per cell or positive cells was observed by fluorescence microscopy (1X71, Olympus, Japan) and quantified by Image J software.

2.10. Co-immunoprecipitation

Primary LSECs were stimulated with aldosterone or co-treated with 3MA for 3 days. IP and immunoblotting (IB) were performed as previously described [16]. The antibodies for IP included anti-Cav1, anti-p62 and anti-ubiquitin; the antibodies for IB included anti-Cav1, anti-p62, anti-ubiquitin, and anti-MR.

2.11. Measurement of intracellular ROS and mitochondrial ROS

Primary LSECs (10^6 cells) were incubated with fluorescence probes DCFH DA (Beyotime, S0033) 10μM for 15 min, and MitoSOX Red Mitochondrial Superoxide Indicator (Thermo, N36008), and then analyzed by flow cytometer (BD, FACSC anto II).

2.12. Small interfering RNA (siRNA) transfection assay

Primary LSECs were transfected with siRNA to knockdown Cav1, according to the manufacturer instructions. The transfection efficiency was 70%. The following Cav1 siRNA sequences were used: sense (5′-GUUGUACCGUGCAUCAAGATT-3′), antisense (5′-UCUUGAUGCACG GUACAACTT-3′).

2.13. q-RT-PCR

Total RNA of cells (10^6) was extracted with Trizol and was reverse transcribed with PrimeScriptTM RT Maseter Mix (Takara, RR036A). Real-time PCR was performed with SYBR Premix Ex TaqTM IIz (Takara, RR820A), using a ROCHE LightCycler® 480. The samples were analyzed using the $2^{-\triangle\triangle Ct}$ method from the Ct values of the respective RNAs (PKG, cGMP, and CYP11B2) relative to the housekeeping gene GAPDH. The following primers were used. cGMP primer (sense: 5′-ATTGGGA TTGTGGGCCATGT-3′; antisense: 5′-TTGTCACGTAGTCGGTGAGC-3′); PKG primer (sense: 5′-CGTTACCCGAGAAGACTCACC-3′; antisense: 5′-GAGACATCATCCAGTCCTCCAA-3′); CYP11B2 primer (sense: 5′-TGCTAAATGGGGCTGACTGG-3′; antisense: 5′-CATCCATGGTAAGGC TCCCTC-3′).

2.14. Extraction of membrane and cytosol protein of primary LSECs

Membrane and Cytosol Protein Extraction Kit (KGP3100-2) was used to extract membrane and cytosol protein of primary LSECs (10^7 cells/group).

2.15. Western blotting

The protein expression in liver tissue or primary LSECs was detected by western blot. The primary antibodies included anti-α-SMA (1:1000), anti-vWF (1:1000), anti-CD31 (1:500), anti-Cav1 (1:1000), anti-MR (1:500), anti-NOX4 (1:1000), anti-p62 (1:1000), anti-LC3 (1:1000), anti-VASP (1:1000), anti-eNOS (1:1000), anti-AMPK (1:1000), anti-ULK1 (1:1000), anti-ubiquitin (1:1000), anti-ATP1B2 (1:1000), anti-GAPDH (1:1000), and anti-β-actin (1:1000). The secondary antibodies were donkey anti-mouse (1:15000, LI-COR biosciences, C40910-04) and goat anti-rabbit (1:15000, LI-COR biosciences, C51007-08).

2.16. Hydrogen peroxide and ATP assay

The H_2O_2 content in cells or liver tissue was measured by a Hydrogen Peroxide Assay Kit (Beyotime, S0038), and the OD value was detected by absorption spectroscopy (562 nm). An ATP Assay Kit (Beyotime, S0026) was used to measure the ATP level in cells, according to the manufacturer's protocol.

2.17. Statistics

The experimental data are reported as the mean ± SD. In statistical analysis of 2 groups, a two-tailed Student's *t*-test was utilized. In analysis of more than 2 groups, ANOVA analyses were performed and analyzed by SPSS17.0 software and $P < 0.05$ was considered significantly.

3. Results

3.1. Elevated aldosterone/MR level with severe oxidation and autophagy in liver sinusoidal endothelium in human liver fibrosis

The area density of Sirius Red staining, the fibrosis level, and the protein expression of α-smooth muscle actin (α-SMA), von Willebrand Factor (vWF), and CD31 in human liver fibrotic tissue were higher than that in the normal group (Fig. 1A–D). Meanwhile, the protein levels of MR, NOX4, and LC3II/I in human fibrotic tissue were also increased (Fig. 1D). The immunofluorescence showed that MR and LC3 were simultaneously highly expressed in CD31-positive or vWF-positive liver sinusoidal endothelium in human liver fibrosis (Fig. 1E). Hence, these suggested that the intra-hepatic aldosterone/MR level was elevated,

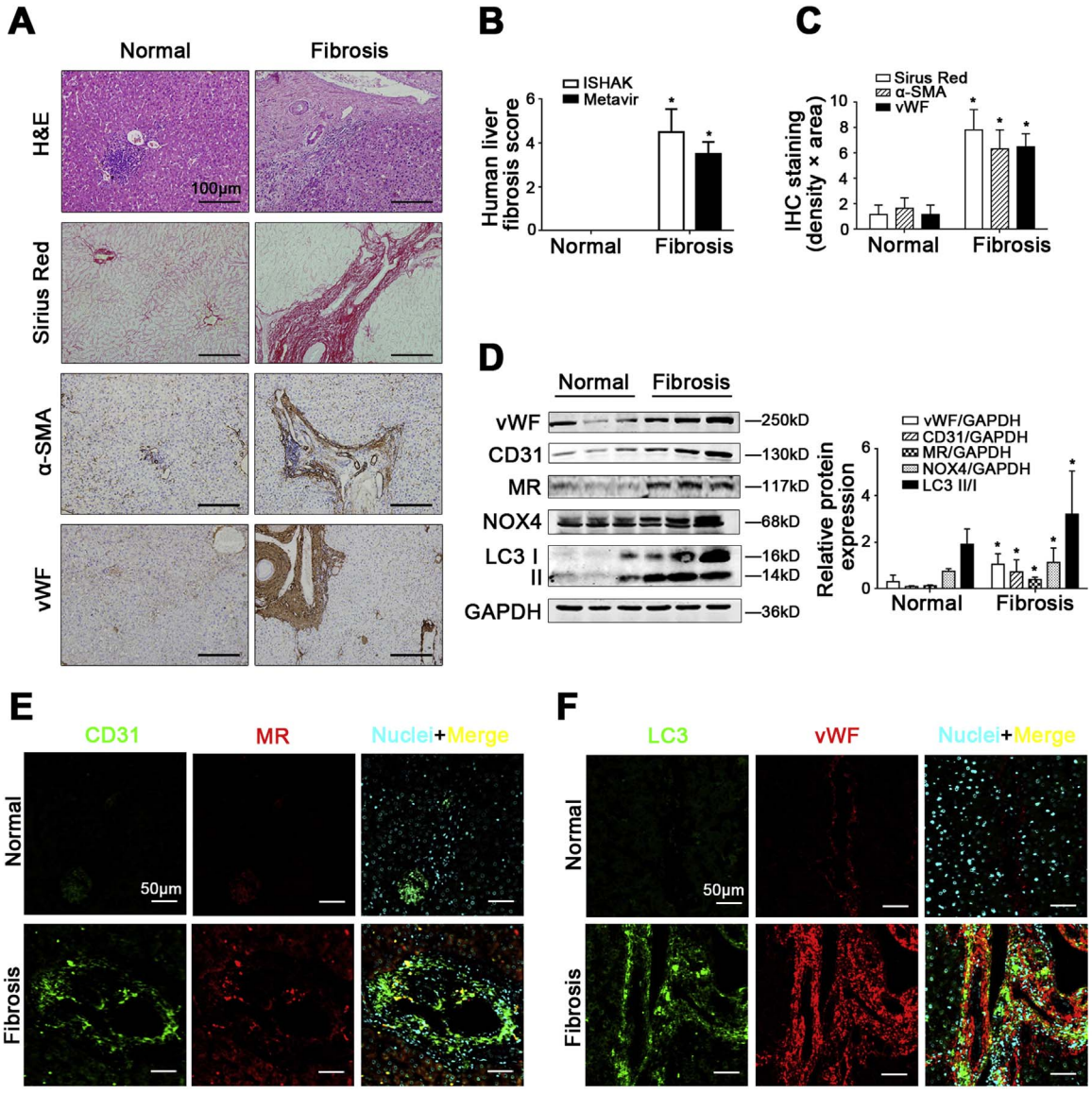

Fig. 1. Elevated aldosterone/MR level with severe oxidation and autophagy in liver sinusoidal endothelium in human liver fibrosis. (**A**) The H & E, Sirius Red, and immunohistochemical staining (IHC) of α-SMA and vWF in liver biopsy specimens (Scale bar: 100 μm). (**B**) The quantified analysis of liver fibrosis with ISHAK and Metavir score. *P < 0.05 versus the normal group. (**C**) The area density of Sirius Red staining and immunohistochemical staining (IHC) of α-SMA and vWF. *P < 0.05 versus the normal group. (**D**) Protein expression of vWF, CD31, MR, NOX4, and LC3 II/I in liver tissue. The relative protein expression is quantified in the graph, right. *P < 0.05 versus the normal group. The co-localization of CD31 with MR (**E**), and the co-localization of LC3 with vWF (**F**) by immunofluorescence (Scale bar: 50 μm).

along with the increase of oxidation and autophagy, in capillarized liver sinusoidal endothelium in human liver fibrosis.

3.2. Antagonizing aldosterone or inhibiting autophagy improves LSECs defenestration in BDL-induced fibrosis

SEM showed that LSECs defenestration occurred on the 18th day in the BDL-induced liver fibrosis (Supplementary Fig. 1A); the protein levels of the NO-dependent pathway in LSECs isolated from the BDL model, such as eNOS and VASP, were decreased, while CD31 was highly expressed from the 18th day to the 28th day (Supplementary Fig. 1B), confirming a pro-fibrotic phenotype transition of LSECs caused by continuous cholestasis. Furthermore, there was a time-dependent up-regulation of serum aldosterone content, along with a high CYP11B2 (aldosterone synthase gene) mRNA level and the increase protein level of MR in LSECs of BDL model (Supplementary Fig. 1B–D), suggesting aldosterone/MR level in LSECs was elevated during BDL-induced LSECs defenestration.

The data of SEM, the protein levels of eNOS and VASP, and the mRNA levels of cGMP and PKG showed that LSECs defenestration and the down-regulation of the NO-dependent pathway were rescued by spironolactone or 3MA treatment (Fig. 2A–C). Additionally, the H_2O_2, mito-ROS and ATP level, the protein levels of MR, Cav1, NOX4 and LC3II/I, the autophagic flux and the data of TEM showed that serious oxidation, mitochondria dysfunction, ATP reduction, and autophagy occurred, along with the elevated MR and Cav1 expression, during LSECs defenestration. However, these effects were improved by spironolactone or 3MA treatment, indicating antagonizing aldosterone or inhibiting autophagy could improve oxidation, autophagy and the NO-dependent pathway to reverse LSECs defenestration (Fig. 2D–H).

Furthermore, antagonizing MR or inhibiting autophagy alleviated the contents of serum ALT and aldosterone, as well as BDL-induced liver

fibrosis (Supplementary Fig. 2).

3.3. Antagonizing aldosterone or inhibiting autophagy relieves LSECs defenestration in hyperaldosteronism mice

To directly unravel the effects of aldosterone on LSECs defenestration and liver fibrosis, we employed the hyperaldosteronism mice model, administered with spironolactone or 3MA. Indeed, the data of SEM and TEM, the protein level of MR and LC3II/I, the H_2O_2 content in liver tissue, as well as the serum aldosterone content showed that in vivo, continuous aldosterone infusion promoted LSECs defenestration, along with the augment of autophagy and oxidation, which could be abirritated by spironolactone or 3MA treatment (Fig. 3). Additionally, the area density of Sirius Red staining, α-SMA protein level in liver tissue, and the serum ALT content, were significantly increased in the hyperaldosteronism mice, which were attenuated by spironolactone or

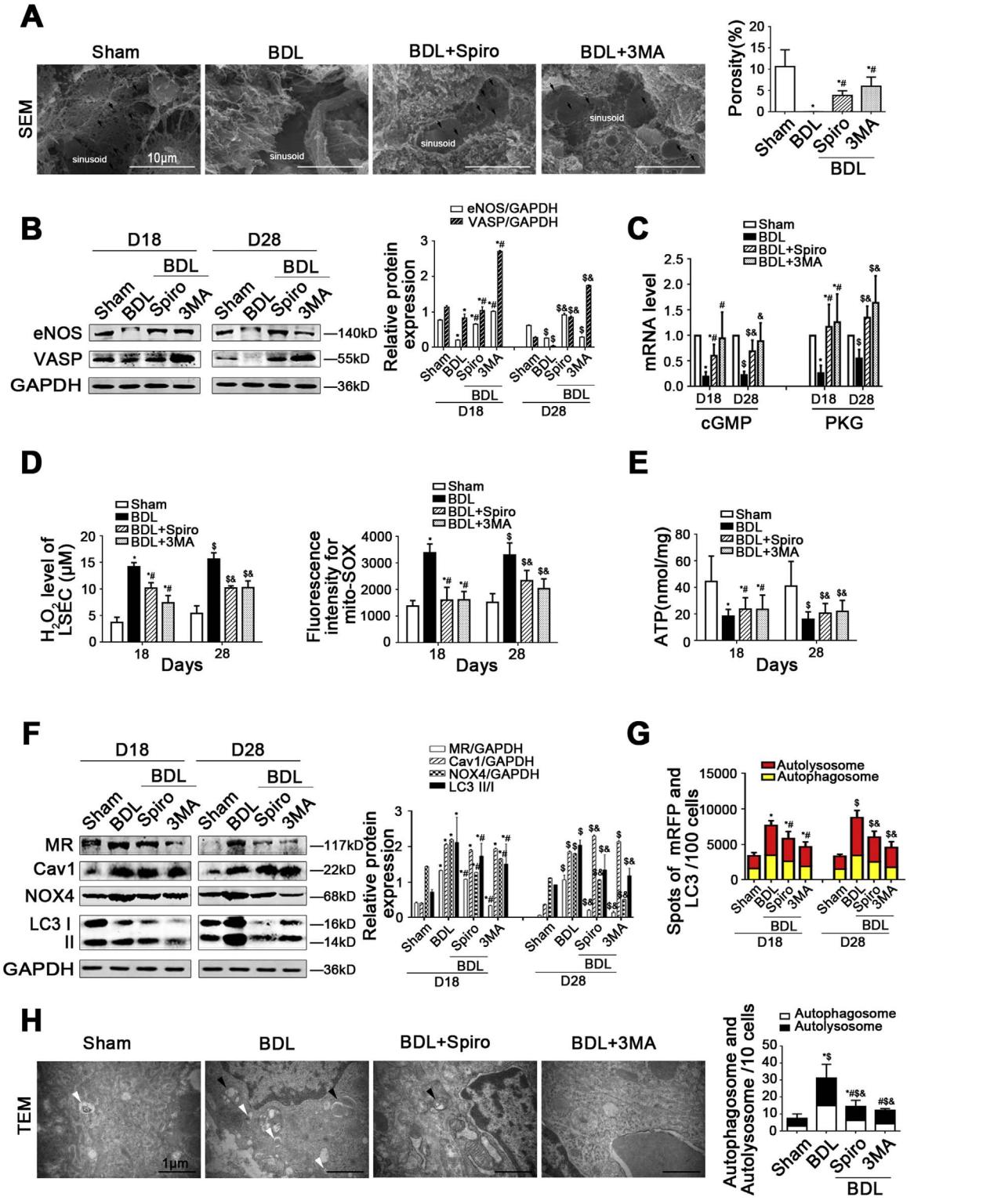

(caption on next page)

Fig. 2. Antagonizing aldosterone or inhibiting autophagy improved LSECs defenestration in BDL-induced fibrosis rats. (**A**) Magnification SEM of liver sinusoidal endothelium in rat liver on Day 18 showing the fenestrae (Scale bar: 10 μm), and quantification of porosity in LSECs of the BDL rat models, right. The black arrows indicate LSECs fenestrae structures. *P < 0.05 versus the sham group; #P < 0.05 versus the BDL group. (**B**) Representative immunoblots of eNOS and VASP in primary LSECs isolated from the BDL rat models. *P < 0.05 versus the sham group on Day 18; #P < 0.05 versus the BDL group on Day 18; $P < 0.05 versus the sham group on Day 28; & P < 0.05 versus the BDL group on Day 28. (**C**) Real-time PCR analysis of cGMP and PKG mRNA levels in primary LSECs isolated from BDL rat models. *P < 0.05 versus the sham group on Day 18; #P < 0.05 versus the BDL group on Day 18; $P < 0.05 versus the sham group on Day 28; & P < 0.05 versus the BDL group on Day 28. (**D**) The H_2O_2 content and mito-ROS in primary LSECs isolated from BDL rat models. *P < 0.05 versus the sham group on Day 18; #P < 0.05 versus the BDL group on Day 18; $P < 0.05 versus the sham group on Day 28; & P < 0.05 versus the BDL group on Day 28. (**E**) The quantification of ATP level in primary LSECs isolated from BDL rat models. *P < 0.05 versus the sham group on Day 18; #P < 0.05 versus the BDL group on Day 18; $P < 0.05 versus the sham group on Day 28; & P < 0.05 versus the BDL group on Day 28. (**F**) Representative immunoblots of MR, Cav1, NOX4 and LC3II/I in primary LSECs. *P < 0.05 versus the sham group on Day 18; #P < 0.05 versus the BDL group on Day 18; $P < 0.05 versus the sham group on Day 28; & P < 0.05 versus the BDL group on Day 28. (**G**) Monitoring of LSECs autophagic flux using a dual fluorescence mRFP-GFP-LC3 marker. Red or yellow represents autolysosomes or autophagosomes respectively, visualized by confocal microscopy. Quantification of autophagic flux (%) in 100 cells was analyzed with Image J software. *P < 0.05 versus autolysosomes and autophagosomes of the sham group on Day 18; #P < 0.05 versus autolysosomes and autophagosomes of the BDL group on Day 18; $P < 0.05 versus autolysosomes and autophagosomes of the sham group on Day 28; & P < 0.05 versus autolysosomes and autophagosomes of the BDL group on Day 28. (**H**) Autophagosomes structures (denoted by white triangles) and autolysosomes structures (denoted by black triangles) in liver sinusoidal endothelium on Day 18 shown in a high-magnification TEM (Scale bar: 1 μm), and bar graphs showing the counts of autophagosomes and autolysosomes, right. *P < 0.05 versus autophagosomes of the sham group; $P < 0.05 versus autolysosomes of the sham group; #P < 0.05 versus autophagosomes of the BDL group; & P < 0.05 versus autolysosomes of the BDL group. n = 6 per group. Spiro: spironolactone. (For interpretation of the references to color in this figure legend, the reader is referred to the web version of this article.)

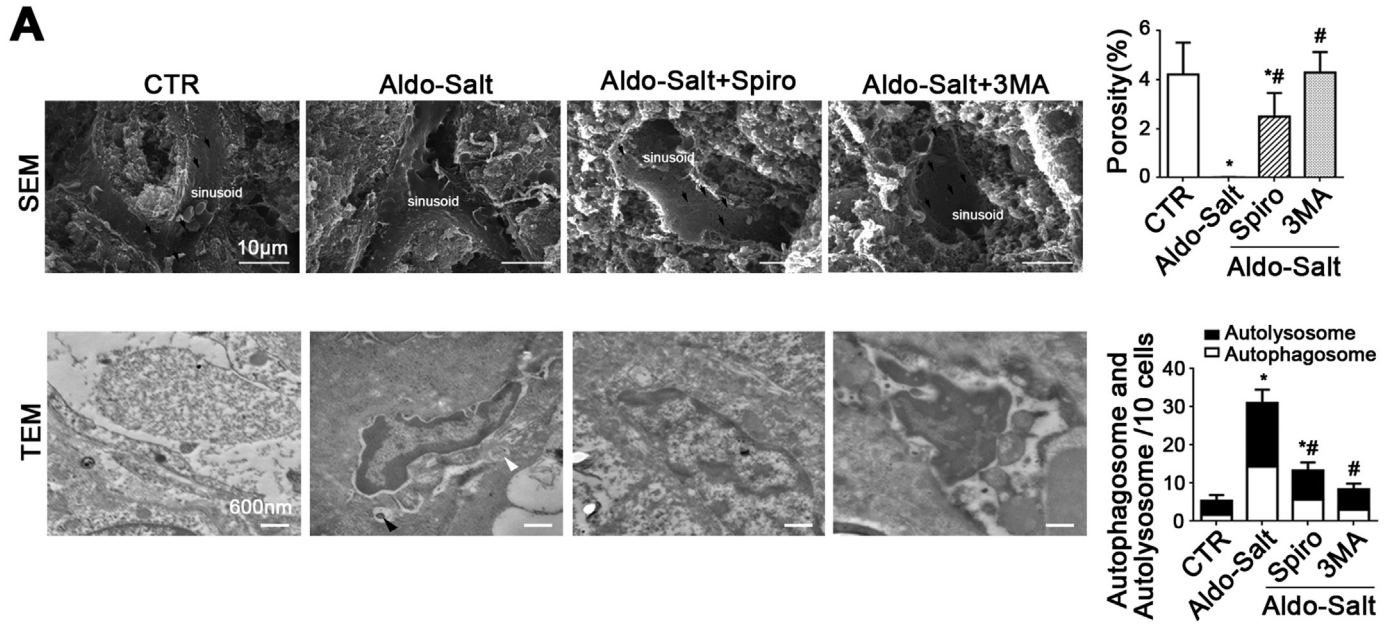

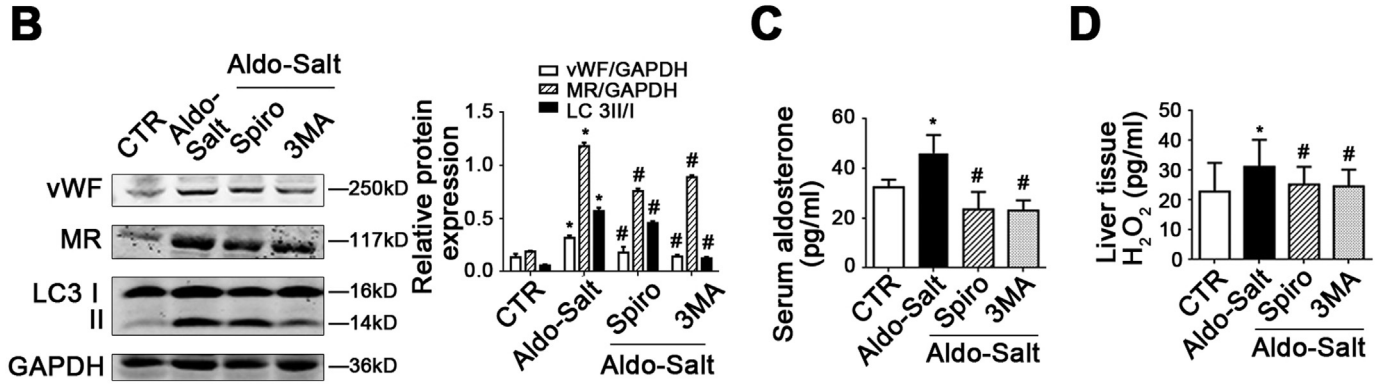

Fig. 3. Antagonizing aldosterone or inhibiting autophagy relieved LSECs defenestration in hyperaldosteronism mice. (**A**) (**Up**) Magnification of SEM of liver sinusoidal endothelium in mice liver showing the fenestrae structures (Scale bar: 10 μm), and quantification of porosity in LSECs, right. The black arrows indicate LSECs fenestrae structures. (**Down**) Autophagosomes structures (denoted by white triangles) and autolysosomes structures (denoted by black triangles) in liver sinusoidal endothelium in mice liver shown with high-magnification TEM (Scale bar: 600 nm), and bar graphs showing the counts of autophagosomes and autolysosomes, right. *P < 0.05 versus the control group; #P < 0.05 versus the Aldo-Salt group. (**B**) Protein levels of vWF, MR, and LC3 II/I analyzed by western blot. The relative protein expression is quantified in the graph, right. *P < 0.05 versus the control group; #P < 0.05 versus the Aldo-Salt group. The serum aldosterone content (**C**) and the H_2O_2 content in liver tissue (**D**). *P < 0.05 versus the control group; #P < 0.05 versus the Aldo-Salt group. n = 9 per group. CTR: control; Aldo: aldosterone; CTR group means 1%NaCl group; Aldo-Salt group means hyperaldosteronism group.

3MA treatment (Supplementary Fig. 3). Hence, these data indicated that in vivo, aldosterone could promote LSECs defenestration and early liver injury via the increase of oxidation and autophagy, which were relieved by antagonizing aldosterone or inhibiting autophagy.

3.4. Acute and chronic aldosterone promotes the AMPK-dependent autophagy during the process of LSECs defenestration

Fenestrae of primary LSECs gradually shrank to disappear during culturing in vitro; while aldosterone-treated LSECs defenestration

occurred on the 3rd day, in advance of the control group (Fig. 4A), suggesting that aldosterone promoted LSECs defenestration in vitro. Moreover, the protein levels of eNOS and VASP showed that there were concentration-dependent and time-dependent down-regulation of the NO-dependent pathway during LSECs fenestrae shrinking, which was exacerbated by aldosterone (Fig. 4B). Interestingly, the data of TEM, the autophagic flux, the protein levels of AMPK, ULK1 and LC3II/I, and the ATP level showed that LSECs fenestrae were shrinking, along with the decrease of ATP and the subsequent augment of the AMPK-ULK1-dependent autophagy, which were aggravated by chronic aldosterone (Fig. 4C–F). Furthermore, the protein levels of p-AMPK (Thr172), p-ULK1 (Ser555), and LC3II/I were increased, along with the decrease of ATP generation by acute aldosterone, suggested the augment of p-AMPK and p-ULK1 activity (Supplementary Fig. 4A, B). Taken together, these data implied that acute and chronic aldosterone triggered the AMPK-ULK1-dependent autophagy to promote LSECs defenestration.

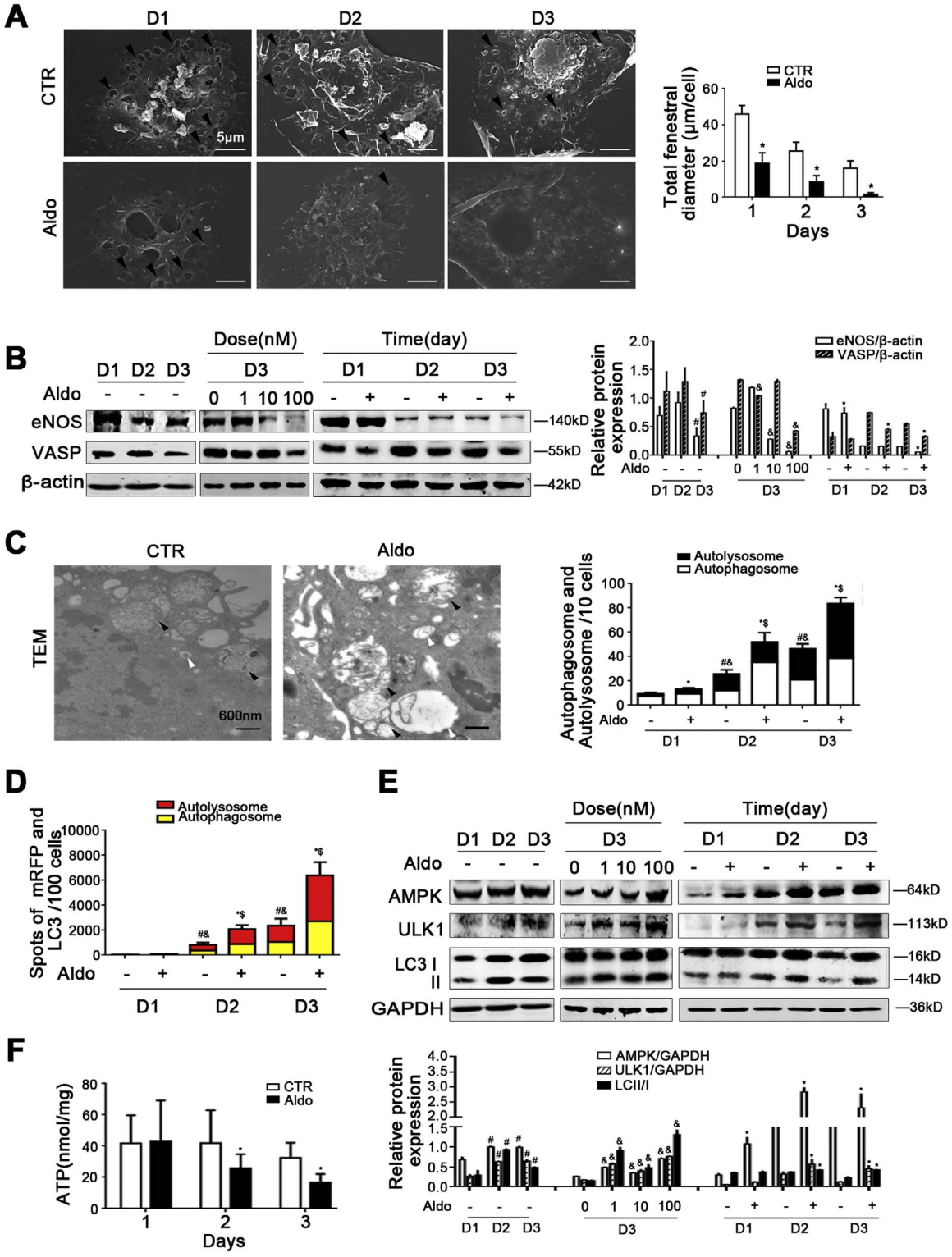

(caption on next page)

Fig. 4. Chronic aldosterone promotes the AMPK-dependent autophagy during the process of LSECs defenestration. Primary rats LSECs, isolated from normal rats and cultured for 3 days in vitro, were treated with aldosterone at the different doses (0, 1, 10, 100 nM) for 3 days or at the dose (100 nM) from Day 1 till Day 3. (**A**) Magnification of SEM of LSECs in CTR and Aldo (100 nM) treatment groups on Day 1, Day 2, and Day 3, revealing the fenestrae structures (Scale bar: 5 μm), and quantification of the total fenestral diameter, right. The black triangles indicate LSECs fenestrae structures. *P < 0.05 versus the concurrent control group. (**B**) Protein levels of eNOS and VASP in primary LSECs analyzed by western blot. The relative protein expression is quantified in the graph, right. #P < 0.05 versus Day 1; & P < 0.05 versus 0 nM; *P < 0.05 versus the concurrent control group. (**C**) Representative TEM images showing autophagosomes structures (denoted by white triangles) and autolysosomes structures (denoted by black triangles) in primary LSECs in CTR and Aldo (100 nM) treatment groups on Day 3 (Scale bar: 600 nm), and bar graphs showing counts of autophagosomes and autolysosomes, right. *P < 0.05 versus the autophagosomes in the concurrent control group; $P < 0.05 versus the autolysosomes in the concurrent control group; #P < 0.05 versus the autophagosomes on Day 1; & P < 0.05 versus the autolysosomes on Day 1. (**D**) Red or yellow represents autolysosomes or autophagosomes respectively, visualized by confocal microscopy. Quantification of autophagic flux (%) in 100 cells was analyzed. *P < 0.05 versus the autophagosomes in the concurrent control group; $P < 0.05 versus the autolysosomes in the concurrent control group; #P < 0.05 versus the autophagosomes on Day 1; & P < 0.05 versus the autolysosomes on Day 1. (**E**) Protein levels of AMPK, ULK1, and LC3 II/I analyzed by western blot. The relative protein expression is quantified in the graph, right. *P < 0.05 versus the autophagosomes in the control group; $P < 0.05 versus the autolysosomes in the control group; #P < 0.05 versus the autophagosomes on Day 1; & P < 0.05 versus the autolysosomes on Day 1. (**F**) The quantification of ATP level in LSECs. *P < 0.05 versus the concurrent control group. (For interpretation of the references to color in this figure legend, the reader is referred to the web version of this article.)

3.5. The AMPK-dependent autophagy is initiated by acute and chronic aldosterone induced-oxidation mediated by Cav1

The protein levels of MR, Cav1 and NOX4, the H_2O_2 and mito-ROS levels in primary rat LSECs showed a concentration-dependent and time-dependent up-regulation of Cav1 expression and oxidative stress by acute and chronic aldosterone treatment (Supplementary Fig. 4C–D, Fig. 5A–C); moreover, the co-IP assays revealed that aldosterone induced enhanced Cav1 co-precipitation with MR (Fig. 5D), suggesting the Cav1 closely interacted with MR to mediate oxidation. Additionally, the NOX4 protein level and the H_2O_2 content in LSECs showed that knockdown of Cav1 by siRNA could reduce aldosterone-initiated oxidation (Fig. 5E–F). These data indicated that aldosterone induced oxidative stress mediated by Cav1.

Furthermore, the H_2O_2, mito-ROS and ATP levels, the protein levels of NOX4, AMPK and LC3II/I and the autophagic flux in primary rat LSECs showed that antagonizing aldosterone (spironolactone) or antioxidants (NAC, TEMPO, mito-TEMPO) could attenuate aldosterone-

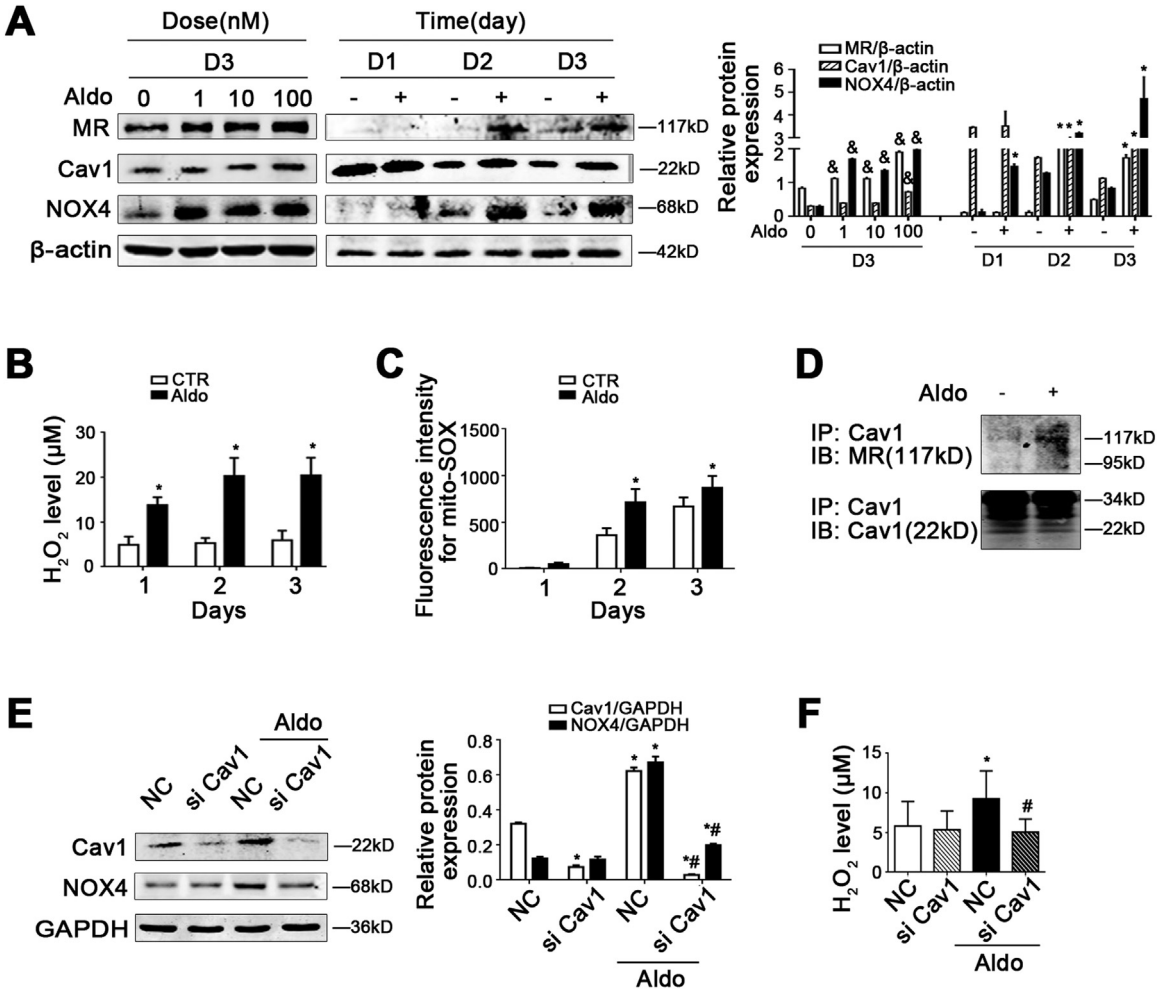

Fig. 5. Aldosterone induced NOX4 and oxidation mediated by Cav1. Primary rats LSECs, isolated from normal rats and cultured for 3 days in vitro, were treated with aldosterone at the different doses (0, 1, 10, 100 nM) for 3 days or at the dose (100 nM) from Day 1 till Day 3. (**A**) Protein levels of MR, Cav1 and NOX4 in primary LSECs analyzed by western blot. The relative protein expression is quantified in the graph, right. & P < 0.05 versus 0 nM; *P < 0.05 versus the concurrent control group. The H_2O_2 content (**B**) and mito-SOX (**C**) in primary LSECs. *P < 0.05 versus the concurrent control group. (**D**) Interaction of Cav1 with MR was detected by the co-IP assay. Cav1 of primary LSECs were individually immunoprecipitated and subjected to immunoblotting analysis as indicated. (**E**) The protein expression of Cav1 and NOX4 in primary LSECs was detected by western blots. The relative protein expression is quantified in the graph, right. *P < 0.05 versus the control group; #P < 0.05 versus NC treated with Aldo. (**F**) The H_2O_2 content of primary LSECs are quantified. *P < 0.05 versus the control group; #P < 0.05 versus NC treated with Aldo.

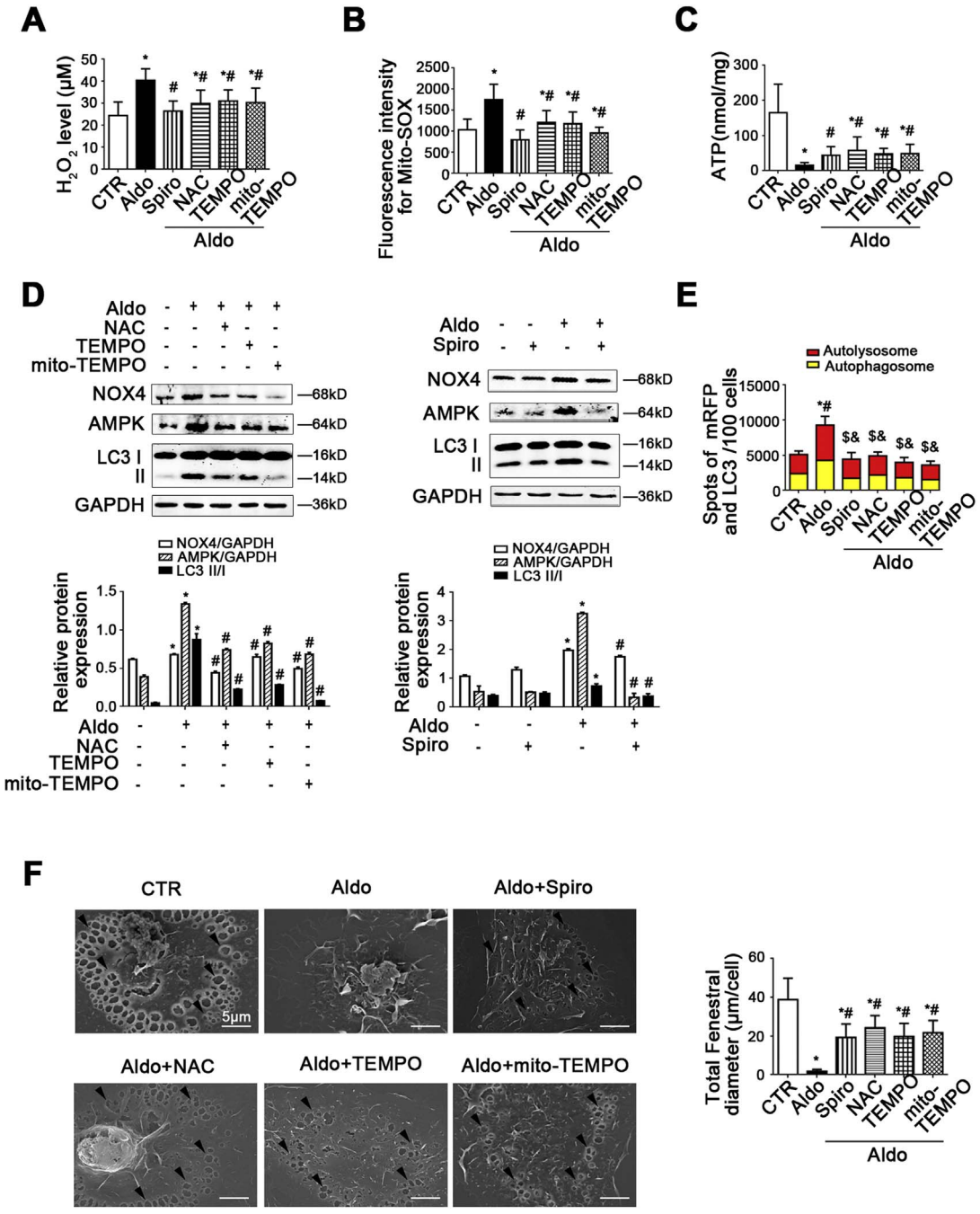

Fig. 6. Spironolactone and antioxidants attenuated the AMPK-dependent autophagy and maintained LSECs fenestrae. Primary rats LSECs, isolated from normal rats and cultured in vitro, were treated with aldosterone (100 nM), and were pre-treated with spironolactone and antioxidants (NAC, TEMPO, or mito-TEMPO) for 3 days. The H_2O_2 content (**A**) and mito-SOX (**B**) in LSECs on Day 3. *P < 0.05 versus the control group; #P < 0.05 versus the Aldo group. (**C**) The quantification of ATP level in LSECs. *P < 0.05 versus the control group; #P < 0.05 versus the Aldo group. (**D**) Representative immunoblots of NOX4, AMPK, and LC3 II/I in LSECs. The relative protein expression is quantified in the graph below. *P < 0.05 versus the control group; #P < 0.05 versus the Aldo group. (**E**) Red or yellow represents autolysosomes or autophagosomes respectively. Quantification of autophagic flux (%) in 100 cells was analyzed. *P < 0.05 versus the autophagosomes in the control group; #P < 0.05 versus the autolysosomes in the control group; $P < 0.05 versus the autophagosomes in the Aldo group; & P < 0.05 versus the autolysosomes in the Aldo group. (**F**) The fenestrae structures of LSECs in CTR, Aldo, and pre-treatment with spirolactone and antioxidants (NAC, TEMPO, or mito-TEMPO) groups, revealed by SEM (Scale bar: 5 μm and 10 μm), and quantification of the total fenestral diameter in LSECs, right. The black triangles indicate LSECs fenestrae structures. *P < 0.05 versus the control group; #P < 0.05 versus the Aldo group. (For interpretation of the references to color in this figure legend, the reader is referred to the web version of this article.)

induced oxidation and improve the ATP production to reduce the AMPK-dependent autophagy (Fig. 6A–E). Indeed, antagonizing aldosterone or antioxidants could maintain fenestrae of aldosterone-treated LSECs (Fig. 6F), indicating that aldosterone-induced oxidation, mediated by Cav1, could initiate the AMPK-dependent autophagy to promote LSECs defenestration.

3.6. Aldosterone-induced the AMPK-dependent autophagy results in LSECs defenestration via inhibiting the NO-dependent pathway

The protein levels of LC3II/I, eNOS and VASP, and the data of SEM in primary rat LSECs showed that autophagy activator (rapamycin) down-regulated the NO-dependent pathway and induced LSECs defenestration; whereas the opposite results were displayed in inhibiting

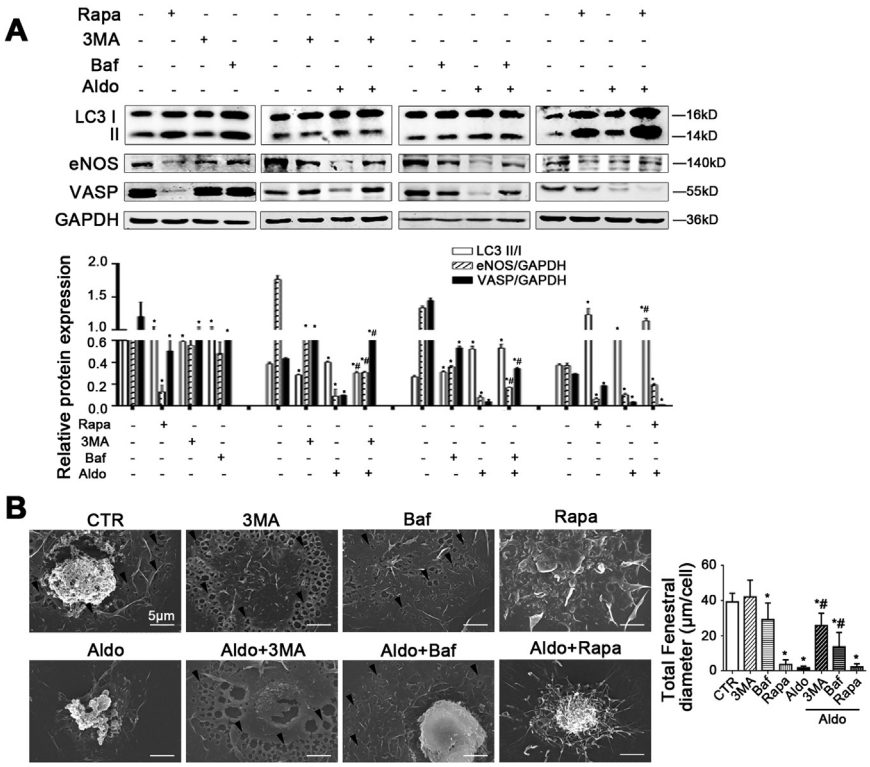

Fig. 7. Aldosterone-induced autophagy resulted in LSECs defenestration via inhibiting the NO-dependent pathway. (**A**) Representative immunoblots of LC3II/I, eNOS, and VASP in primary LSECs, pre-treated with autophagy regulators (rapamycin, 3MA, or bafilomycin). The relative protein expression is quantified in the graph below. *P < 0.05 versus the control group; #P < 0.05 versus the Aldo group. (**B**) Magnification SEM of LSECs in eight groups (CTR, 3MA, Baf, Rapa, Aldo, Aldo + 3MA, Aldo + Baf, Aldo + Rapa) on Day 3, revealing the fenestrae structures (Scale bar: 5 μm), and quantification of the total fenestral diameter in LSECs, right. The black triangles indicate LSECs fenestrae structures. *P < 0.05 versus the control group; #P < 0.05 versus the Aldo group. Rapa: rapamycin; Baf: bafilomycin A1.

autophagy treatment (3MA or bafilomycin) (Fig. 7A–B).

Additionally, in aldosterone-treated LSECs, the ROS, mito-ROS and the NOX4 protein level were reduced by pre-treatment with 3MA, bafilomycin or rapamycin, suggesting that either inhibiting or enhancing autophagy could improve oxidative stress induced by aldosterone (Supplementary Fig. 5). Despite the decrease of oxidation, pre-treatment with rapamycin could induce the AMPK-dependent autophagy, the down-regulation of the NO-dependent pathway and LSECs defenestration; while these effects were reversed by pre-treatment with 3MA or bafilomycin (Supplementary Fig. 5D, Fig. 7A–B). These data suggested that the AMPK-dependent autophagy induced by aldosterone promoted LSECs defenestration.

3.7. Aldosterone induces selective autophagic degradation and redistribution of Cav1, and promotes F-actin remodeling

There was a time-dependent down-regulation of the Cav1 protein level, along with the augment of autophagy during LSECs fenestrae shrinking from the 1st day to the 3rd day in vitro (Supplementary Fig. 6A). Furthermore, enhancing autophagy (rapamycin), which promoted LSECs defenestration, could reduce the Cav1 protein level; whereas the opposite results were displayed in the 3MA or bafilomycin group (Fig. 8A). Additionally, the immunofluorescence showed that Cav1 co-localized with LC3 in the perinuclear area in the autophagy activator (rapamycin) treatment group, compared to the control group (Supplementary Fig. 6B). Furthermore, the Cav1 protein level in membrane and cytoplasm showed that rapamycin reduced Cav1 protein expression both in membrane and cytoplasm due to enhanced autophagy (Fig. 8C). These results indicated that autophagy could promote degradation of Cav1.

Interestingly, compared with the control group, aldosterone enhanced the co-localization of Cav1 with LC3 in the perinuclear area, which was reversed by the pre-treatment with 3MA or bafilomycin (Supplementary Fig. 6B), suggesting the redistribution of Cav1; the co-IP assay revealed that aldosterone enhanced the co-precipitation of Cav1 with p62 and ubiquitin due to enhancing autophagy; in contrast, 3MA inhibited autophagy to break this interaction (Fig. 8B). Additionally, the Cav1 protein level in membrane and cytoplasm showed that aldosterone increased membranal Cav1 level but decreased cytoplasmic Cav1 level. These suggested that aldosterone induced Cav1-related selective autophagy and the redistribution of Cav1 (Fig. 8C).

Furthermore, the immunofluorescence showed that Cav1 co-localized with ubiquitin and F-actin in the perinuclear area of LSECs in the rapamycin- or aldosterone-treated group; in contrast, less co-localization of Cav1 with ubiquitin and F-actin were displayed in the 3MA- or bafilomycin-treated group, and Cav1 and F-actin were uniformly distributed throughout the cytoplasm (Fig. 8D), suggesting remodeling and redistribution of F-actin triggered by aldosterone through the selective autophagy and redistribution of Cav1 (Fig. 9).

Hence, aldosterone exacerbated Cav1-related autophagy in the perinuclear area to promote F-actin remodeling and LSECs defenestration, which were recovered by inhibition of autophagy.

4. Discussion

In the present study, we demonstrated for the first time that Cav1-related autophagy initiated by aldosterone-induced oxidation promotes LSECs defenestration. The principal findings obtained include the followings: (1) *In vivo*, spironolactone or 3MA could improve NOX4- and mitochondria-mediated oxidation, and inhibit autophagy to alleviate LSECs defenestration and liver fibrosis. (2) Acute and chronic aldosterone increases NOX4- and mitochondria- derived oxidative stress mediated by Cav1, and subsequently initiates the AMPK-dependent autophagy. (3) Aldosterone induces the selective autophagy and redistribution of Cav1 to promote F-actin remodeling. (4) Aldosterone, with pro-oxidation and pro-autophagy capabilities, inhibits the NO-dependent pathway to promote LSECs defenestration.

As we know, reactive oxygen species (ROS) plays a key role in pathogenesis of liver fibrosis. The mitochondrial respiratory chain and the NADPH oxidases (NOXs), which are two primary cellular sources of ROS, generate superoxide (O_2^-) and H_2O_2 [17,18]. NOXs-mediated ROS plays a critical role in HSCs activation and liver fibrosis, suggesting its potential role as a pharmacological target for anti-fibrotic therapy [19].

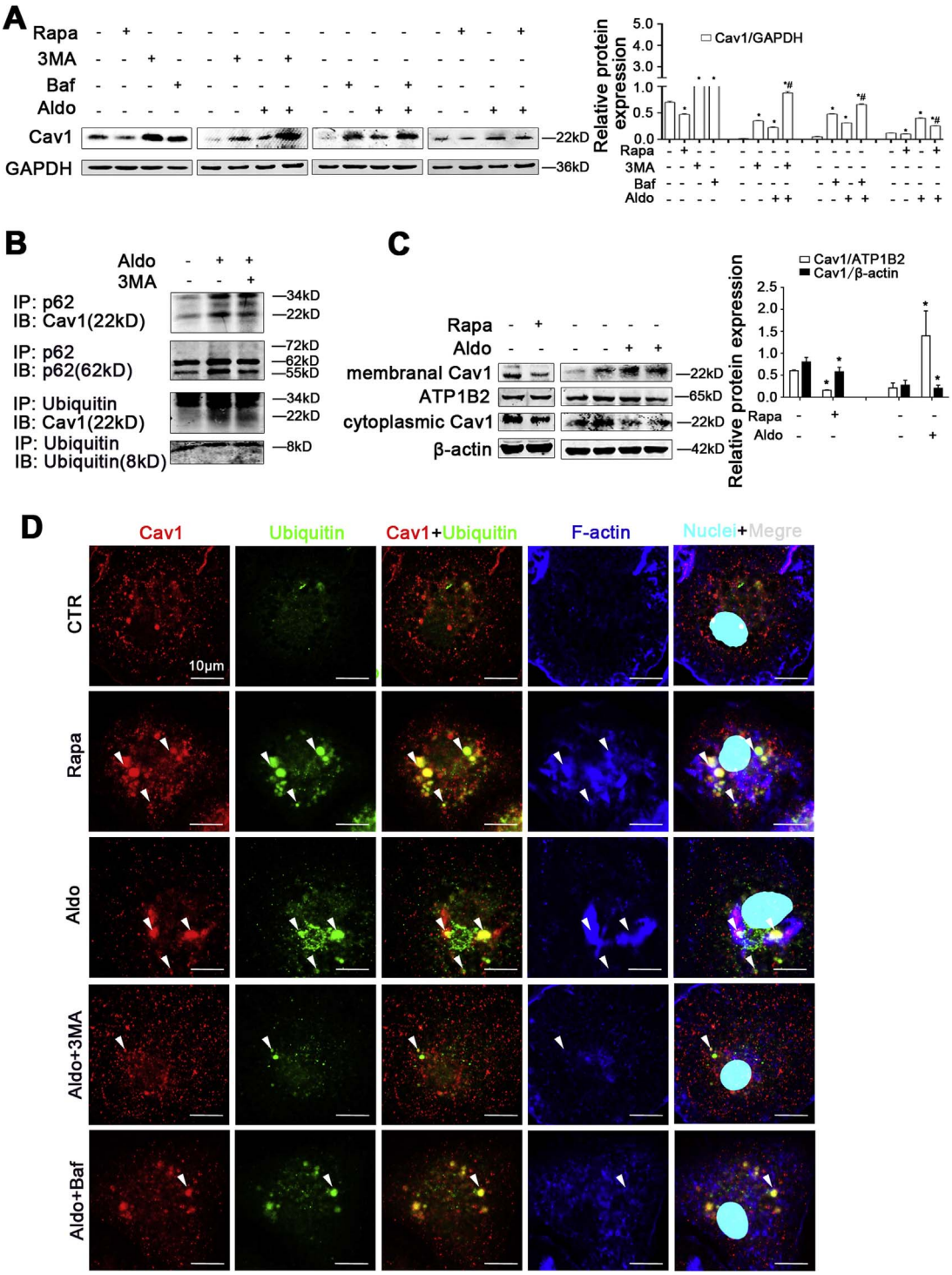

Fig. 8. Aldosterone induced selective autophagic degradation and redistribution of Cav1 to promote F-actin remodeling. (**A**) Representative immunoblots of Cav1 in primary LSECs, pre-treated with autophagy regulators (rapamycin, 3MA, or bafilomycin). The relative protein expression is quantified in the graph, right. *P < 0.05 versus the control group; #P < 0.05 versus the Aldo group. (**B**) Interaction of Cav1 with p62 and ubiquitin was detected by co-IP. P62 and ubiquitin of primary LSECs were individually immunoprecipitated and subjected to immunoblotting analysis as indicated. (**C**) Representative immunoblots of Cav1 and ATP1B2 in membrane, as well as Cav1 and β-actin in cytoplasm in primary LSECs, treated with autophagy regulators (rapamycin, 3MA, or bafilomycin) and aldosterone on Day 3. *P < 0.05 versus the control group. (**D**) The co-localization of Cav1 (red) with ubiquitin (green) and F-actin (blue) in LSECs of the five groups (CTR, Rapa, Aldo, Aldo + 3MA, and Aldo + Baf), shown by immunofluorescence. Scale bar: 10 μm. (For interpretation of the references to color in this figure legend, the reader is referred to the web version of this article.)

Additionally, NOX4 mediates distinct profibrogenic actions in HSCs in the liver [20]. What's more, parts of ROS are usually released by the mitochondrial respiratory chain in the liver. Mitochondrial reactive oxygen species also play an important role in liver fibrosis and mitochondria-targeted antioxidants attenuates liver fibrosis [21].

It has been evidenced that local tissue based aldosterone promotes liver fibrogenesis via its pro-oxidation. Our previous study found that aldosterone induced NOX4-mediated oxidative stress to activate HSCs and promote liver fibrosis, which could be attenuated by aldosterone antagonist spironolactone [22]. And spironolactone has been clinically utilized to attenuate portal hypertension [23]. Furthermore, our present study found that continuous aldosterone could directly induce early

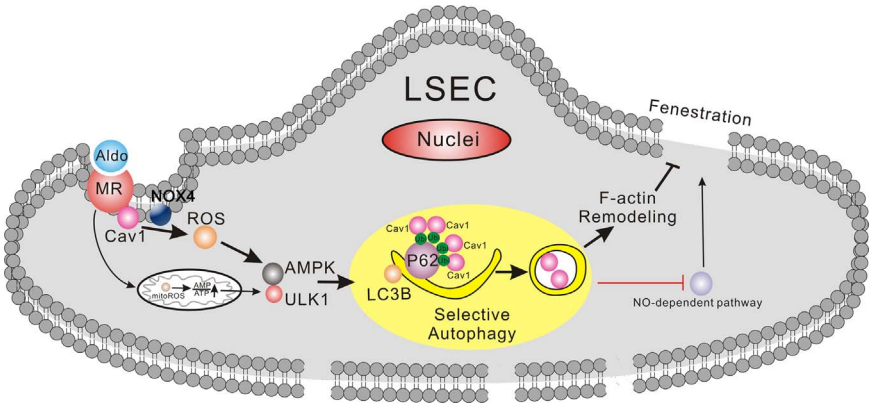

Fig. 9. A schematic view of major signal transduction pathways involved in the conclusion that aldosterone-induced autophagic degradation of Cav1 promotes defenestration of liver sinusoidal endothelial cells via F-actin remodeling and inhibiting the NO-dependent pathway.

liver fibrosis through NOXs- and mitochondria-mediated ROS, which could improve by spironolactone. Hence, aldosterone is a promising drug target for liver fibrosis.

In addition, aldosterone promotes LSECs defenestration via its pro-oxidation and pro-autophagy. *In vivo*, we found that the serum aldosterone content and MR protein level of LSECs were increased, along with the increase of oxidation and autophagy in LSECs during the process of defenestration in BDL-induced liver fibrosis, which were recovered by antagonizing aldosterone (spironolactone) or inhibiting autophagy (3MA). The hyperaldosteronism model further demonstrated that in vivo, continuous aldosterone infusion could promote LSECs defenestration via oxidative stress and enhanced autophagy, which were relieved by spironolactone or 3MA.

However, how pro-oxidation and pro-autophagy, induced by aldosterone, impact on LSECs defenestration remains unknown. Firstly, it's reported that NOXs- or mitochondria-mediated oxidative stress may cause endothelial dysfunction [19,24,25]. Our present study found that in vitro, both acute and chronic aldosterone could induce NOX4- and mitochondria-mediated oxidative stress during the process of LSECs defenestration, which could attenuate by spironolactone, antioxidants, and autophagy inhibitors (3MA and bafilomycin). These suggest that aldosterone-induced oxidation could promote LSECs defenestration.

Next, we explored the influence of autophagy-initiated by aldosterone on LSECs defenestration. Interestingly, the literatures about the effects of autophagy on liver fibrosis are diverse [3,4], maybe due to the roles of autophagy in liver fibrosis varying with intra-hepatic cell type. Recently, autophagy was reported to modulate the phenotype of LSECs and protect against acute liver injury induced by I/R [5]. Here, we found that the AMPK-dependent autophagy was increased, along with the down-regulation of the NO-dependent pathway during LSECs fenestrae shrinking in vitro; while autophagy activator (rapamycin) could aggravate these effects. However, autophagy inhibitors (3MA or bafilomycin) could maintain LSECs fenestrae and improve the NO-dependent pathway. These suggest that the AMPK-dependent autophagy induces LSECs defenestration. In addition, we found that aldosterone promoted LSECs defenestration and the reduction of the NO-dependent pathway, along with enhancing autophagy and oxidation. So, how does aldosterone affect on LSECs defenestration via its pro-oxidation and pro-autophagy capabilities? It was reported that ROS and depletion of ATP could directly induce autophagy via the AMPK-ULK1 pathway [26]. The present study showed that both acute and chronic aldosterone led to a persistent oxidation and the reduction of ATP generation, and subsequence the activation of the AMPK-ULK1-dependent autophagy, so as to LSECs defenestration and the reduction of NO-dependent pathway, which were attenuated by sprionolactone, antioxidants or autophagy inhibitors. Hence, aldosterone-induced oxidation and dysfunction of ATP generation initiate autophagy via the AMPK-ULK1 pathway to promote LSECs defenestration.

As a crucial factor, Cav1 connects with oxidation and autophagy. Cav1 is a structural protein on the plasma membrane of fenestrae as well as vesicles in LSECs [27]. In membrane, Cav1 is necessary for caveolae biogenesis, which is a functional small invagination, interacting with various enzymes and receptors, and mediating a rapid signaling cascade; on the other hand, intracellular Cav1 also assists in activation to signal transduction and trafficking [10]. The opinions about the effects of Cav1 on LSECs fenestrae and capillarization are controversial. Carlos Fernandez-Hernando, et al. demonstrate for the first time that Cav1 changes the porosity of the LSECs and reduces the diameter of fenestrations; while the genetic ablation of Cav1 induces defenestration in LSECs [28]. But others argued that the LSECs fenestration in Cav1 knockout mice had no change in normal condition [29]. It seems that Cav1 is not so much essential to maintain the fenestrae of LSECs. But here, we demonstrated for the first time that Cav1 is indeed a multifunctional signaling hub that mediate aldosterone-induced oxidation and autophagy to regulate LSECs defenestration.

In caveolae, Cav1 plays an important role in mediating aldosterone-induced oxidation. A variety of ROS, such as superoxide and H_2O_2, in caveolae or other microdomains, play a crucial role in cell signaling [30]. The literatures about the effects of Cav1 on oxidation are complex. It's reported that Cav1 is a negative regulator of NOXs-derived ROS through direct binding and alteration of expression [31]. The knockdown or knockout of Cav1 has been shown to increase ROS levels in the vasculature and can promote cardiovascular diseases. [32]. The decrease of Cav1 level could activate the aldosterone/MR signaling on the pathways of glycemia, dyslipidemia, and resistin [33]. However, Cav1 interacts with MR and form a MR/Cav1 complex, which mediates a rapid signaling cascade of oxidation initiated by aldosterone [10]. Aldosterone induced more abundant of MR/Cav1 complexes to interacted with NOX4, leading to oxidation [34]. These indicate that the effects of Cav1 on redox modification may be different with a variety of cell types. Our present study demonstrated for the first time that aldosterone induced the augment of membranal Cav1, which was enhanced the co-precipitation with MR, leading to NOX4- or mitochondrial-derived oxidative stress in LSECs, and subsequence the triggering of the AMPK-dependent autophagy. Furthermore, knockdown of Cav1 could attenuate NOX4-and mitochondrial-mediated ROS induced by aldosterone.

In addition, intracellular Cav1 participates in the regulation of aldosterone-induced autophagy. Song et al. [11] found that Cav1 mediated autophagy of intestinal epithelial cells via triggering NOX dependent oxidation. Besides, intracellular Cav1 also mediates autophagy through the regulation of ATG12-ATG5 system and energetic generation. Chen et al. [12] reported that Cav1 could interact with ATG12-ATG5 system to suppress autophagy in lung epithelial cells. Ha et al. [35] described that depletion of Cav1 led to reduction of GLUT3 related glucose uptake and ATP generation, activating the AMP-ATP ratio/AMPK pathway to induce autophagy and diminish cellular metabolism, which in turn reinforced cytosolic AMPK-dependent autophagy. Interestingly, our data firstly showed that there was a time-dependent down-regulation of the Cav1 protein level, along with the augment of

autophagy during LSECs fenestrae shrinking. Enhancing autophagy (rapamycin), which promoted LSECs defenestration, could reduce both membranal and intracellular Cav1 protein expression; whereas the opposite results were displayed in the 3MA or bafilomycin group due to inhibiting autophagy. Moreover, the enhanced co-localization of Cav1 with LC3 in the rapamycin group directly showed that the increase of autophagy promoted the redistribution of Cav1 to autophagosome (denoted by LC3) in the perinuclear area of LSECs. These indicate that autophagy could initiate degradation of Cav1 to promote LSECs defenestration. It is noteworthy that more Cav1 co-localized with LC3 or ubiquitin in perinuclear area of LSECs in aldosterone-treated group, which indicated that aldosterone induced intracellular Cav1 redistribute to autophagosome in LSECs; meanwhile aldosterone enhanced the co-immunoprecipitation of Cav1 with p62 and ubiquitin due to enhancing autophagy, whereas 3MA inhibited autophagy to break this interaction. These suggest that aldosterone induced Cav1-related autophagy in cytoplasm. Additionally, in spite of the increase of membranal Cav1 expression, aldosterone decreased cytoplasmic Cav1 level due to enhanced autophagy. These indicate the selective autophagic degradation and redistribution of intracellular Cav1 were induced by aldosterone.

Furthermore, it has been confirmed that F-actin, being part of the cytoskeleton around fenestrae, modulates contraction of fenestrae [13], whose remodeling may facilitate defenestration. Besides, Lee et al. [14] reported that autophagy could assemble an F-actin network and facilitated remodeling, indicating that autophagy contributes to F-actin remodeling and subsequent fenestrae contraction. Here we found that the immunofluorescence showed that rapamycin or aldosterone increased the co-localization of Cav1 with ubiquitin and F-actin in the perinuclear area of LSECs due to enhancing autophagy, which was reversed by autophagy inhibitor (3MA or bafilomycin). Hence, we suspected that Cav1-related autophagy participates in LSECs defenestration through regulating F-actin remodeling, which were aggravated by aldosterone.

As mentioned above, it seems that Cav1 plays a dual role in regulation of defenestration in aldosterone-treated LSECs: on the one hand, in plasma membrane, NOX4- and mitochondria-derived oxidation, mediated by MR/Cav1 complex, lead to depletion of ATP and subsequent autophagy, which may impair the fenestrae; on the other hand, in cytoplasm, the autophagic degradation and redistribution of Cav1 promote F-actin remodeling and LSECs defenestration.

Finally, we focus on the effects of autophagy and oxidation on the NO-dependent pathway. There are two kinds of signaling pathways to maintain LSECs differentiation status: the NO-dependent pathway (namely the NO/eNOS/sGC/cGMP/PKG/VASP pathway) and the NO-independent pathway [36,37]. The literatures indicate aldosterone negatively regulates the NO/eNOS signaling via its pro-oxidation. Toda et al. [38] demonstrated that oxidative stress, induced by chronic exposure to aldosterone, leads to endothelial dysfunction and vasoconstriction because of decline and degradation of NO synthesis. Additionally, acute exposure to aldosterone induced serious oxidation in human umbilical vein endothelial cells (HUVECs), along with the reduction of the eNOS dimmer/ monomer ratio [39]. Activation of MR signaling contributes to eNOS uncoupling and the vascular dysfunction; while spironolactone restored NO bioavailability [40]. Here, our data showed that the NO-dependent pathway of LSECs was down-regulated by aldosterone treatment or BDL, which was reversed by spironolactone or antioxidants. Hence, oxidation mediates aldosterone-induced defenestration via inhibiting the NO-dependent pathway. Besides, Sarkar et al. [41] reported that NO could negatively regulate autophagosome synthesis and autophagosome-lysosome fusion, while an eNOS inhibitor (L-NAME) induced autophagy. Rapamycin is associated with the reduction of eNOS, affecting vasomotion [42]. Hence autophagy negatively interacts with the NO/eNOS signaling. We also found that rapamycin inhibited the NO-dependent pathway; while autophagy inhibitors up-regulate the NO-dependent pathway to maintain LSECs fenestrae. Hence, we demonstrated that aldosterone-induced autophagy promoted LSECs defenestration via inhibiting the NO/eNOS/cGMP/PKG pathway.

However, there are some limitations to the present study. The role of autophagy-induced Cav1 redistribution to perinuclear area of LSECs in defenestration needs further investigation. Moreover, we still have not clearly revealed the mechanism underlying Cav1-related selective autophagy regulating F-actin remodeling and the NO-dependent pathway.

In summary, Cav1-related autophagy initiated by aldosterone-induced oxidation promotes LSECs defenestration.

5. Conclusion

Cav1-related selective autophagy initiated by aldosterone-induced oxidation promoted LSECs defenestration via activating the AMPK-ULK1 pathway and inhibiting the NO-dependent pathway. Inhibition of LSECs autophagy is a promising strategy for preventive treatment of sinusoidal capillarization.

Conflicts of interest

No potential conflicts of interest were disclosed.

Acknowledgements and funding

The authors are much grateful to Prof. Pingsheng Wu, Prof. Zhenshu Zhang, and Prof. Xishan Yang for essential helps in this study. This study was funded by the National Natural Science Foundation of China (81270520 and 81670556), Guangzhou Pilot Project of Clinical and Translational Research Center (early gastrointestinal cancers, No. 7415696196402), and Guangdong Provincial Bio-engineering Research Center for Gastroenterology Disease **(No. 00212320255326091)**.

Appendix A. Supporting information

Supplementary data associated with this article can be found in the online version at http://dx.doi.org/10.1016/j.redox.2017.07.011.

References

[1] B. Levine, G. Kroemer, Autophagy in the pathogenesis of disease, Cell 132 (2008) 27–42.
[2] M. Dewaele, H. Maes, P. Agostinis, ROS-mediated mechanisms of autophagy stimulation and their relevance in cancer therapy, Autophagy 6 (2010) 838–854.
[3] R.H. Bhogal, C.J. Weston, S.M. Curbishley, D.H. Adams, S.C. Afford, Autophagy: a cyto-protective mechanism which prevents primary human hepatocyte apoptosis during oxidative stress, Autophagy 8 (2012) 545–558.
[4] L.F. Thoen, E.L. Guimarães, L. Dollé, I. Mannaerts, M. Najimi, E. Sokal, et al., A role for autophagy during hepatic stellate cell activation, J. Hepatol. 55 (2011) 1353–1360.
[5] S. Guixé-Muntet, F.C. de Mesquita, S. Vila, V. Hernández-Gea, C. Peralta, J.C. García-Pagán, et al., Cross-talk between autophagy and KLF2 determines endothelial cell phenotype and micro-vascular function in acute liver injury, J. Hepatol. 66 (2017) 86–94.
[6] N.J. Brown, Contribution of aldosterone to cardiovascular and renal inflammation and fibrosis, Nat. Rev. Nephrol. 9 (2013) 459–469.
[7] N. Queisser, K. Happ, S. Link, D. Jahn, A. Zimnol, A. Geier, et al., Aldosterone induces fibrosis, oxidative stress and DNA damage in livers of male rats independent of blood pressure changes, Toxicol. Appl. Pharmacol. 280 (2014) 399–407.
[8] M. Bai, R. Che, Y. Zhang, Y. Yuan, C. Zhu, G. Ding, et al., Reactive oxygen species-initiated autophagy opposes aldosterone-induced podocyte injury, Am. J. Physiol. Ren. Physiol. 13 (2016).
[9] Y. Yuan, X. Xu, C. Zhao, M. Zhao, H. Wang, B. Zhang, et al., The roles of oxidative stress, endoplasmic reticulum stress, and autophagy in aldosterone/mineralocorticoid receptor-induced podocyte injury, Lab. Investig. 95 (2015) 1374–1386.
[10] R. Baudrand, L.H. Pojoga, J.R. Romero, G.H. Williams, Aldosterone's mechanism of action: roles of lysine specific demethylase 1, caveolin and striatin, Curr. Opin. Nephrol. Hypertens. 23 (2014) 32–37.
[11] E.J. Song, S.J. Lee, H.S. Lim, J.S. Kim, K.K. Jang, S.H. Choi, et al., Vibrio vulnificus VvhA induces autophagy-related cell death through the lipid raft-dependent c-Src/NOX signaling pathway, Sci. Rep. 6 (2016) 27080.
[12] Z.H. Chen, J.F. Cao, J.S. Zhou, H. Liu, L.Q. Che, K. Mizumura, et al., Interaction of

caveolin-1 with ATG12-ATG5 system suppresses autophagy in lung epithelial cells, Am. J. Physiol. Lung Cell Mol. Physiol. 306 (2014) L1016–L1025.
[13] F. Braet, E. Wisse, Structural and functional aspects of liver sinusoidal endothelial cell fenestrae: a review, Comp. Hepatol. 1 (2002) 1.
[14] J.Y. Lee, H. Koga, Y. Kawaguchi, W. Tang, E. Wong, Y.S. Gao, et al., HDAC6 controls autophagosome maturation essential for ubiquitin-selective quality-control autophagy, EMBO J. 29 (2010) 969–980.
[15] F. Braet, R. De Zanger, T. Sasaoki, M. Baekeland, P. Janssens, B. Smedsrød, et al., Assessment of a method of isolation, purification and cultivation of rat liver sinusoidal endothelial cells, Lab. Investig. 70 (1994) 944–952.
[16] K. Nakahira, H.P. Kim, X.H. Geng, A. Nakao, X. Wang, N. Murase, et al., Carbon monoxide differentially inhibits TLR signaling pathways by regulating ROS-induced trafficking of TLRs to lipid rafts, J. Exp. Med. 203 (2006) 2377–2389.
[17] M.P. Murphy, How mitochondria produce reactive oxygen species, Biochem. J. 417 (2009) 1–13.
[18] K. Bedard, K.H. Krause, The NOX family of ROS-generating NADPH oxidases: physiology and pathophysiology, Physiol. Rev. 87 (2007) 245–313.
[19] Y.H. Paik, D.A. Brenner, NADPH oxidase mediated oxidative stress in hepatic fibrogenesis, Korean J. Hepatol. 17 (2011) 251–257.
[20] Y.H. Paik, J. Kim, T. Aoyama, S. De Minicis, R. Bataller, D.A. Brenner, Role of NADPH oxidases in liver fibrosis, Antioxid. Redox Signal 20 (2014) 2854–2872.
[21] H. Rehman, Q. Liu, Y. Krishnasamy, Z. Shi, V.K. Ramshesh, K. Haque, et al., The mitochondria-targeted antioxidant MitoQ attenuates liver fibrosis in mice, Int. J. Physiol. Pathophysiol. Pharmacol. 8 (2016) 14–27.
[22] W.Y. Zhang, Y. Li, T. Li, Z.W. Ning, W. Li, X. Li, Aldosterone antagonist inhibits fibrosis-induced NOX4 protein expression in hepatic cells and tissues of rats, Zhonghua Gan Zang Bing. Za Zhi 21 (2013) 519–523.
[23] I. Sungaila, W.R. Bartle, S.E. Walker, C. DeAngelis, J. Uetrecht, C. Pappas, et al., Spironolactone pharmacokinetics and pharmacodynamics in patients with cirrhotic ascites, Gastroenterology 102 (1992) 1680–1685.
[24] D. Graham, N.N. Huynh, C.A. Hamilton, E. Beattie, R.A. Smith, H.M. Cochemé, et al., Mitochondria-targeted antioxidant MitoQ10 improves endothelial function and attenuates cardiac hypertrophy, Hypertension 54 (2009) 322–328.
[25] S.F. Bronk, G.J. Gores, Acidosis protects against lethal oxidative injury of liver sinusoidal endothelial cells, Hepatology 14 (1991) 150–157.
[26] R.A. Sinha, B.K. Singh, J. Zhou, Y. Wu, B.L. Farah, K. Ohba, et al., Thyroid hormone induction of mitochondrial activity is coupled to mitophagy via ROS-AMPK-ULK1 signaling, Autophagy 11 (2015) 1341–1357.
[27] M. Ogi, H. Yokomori, M. Oda, K. Yoshimura, M. Nomura, S. Ohshima, et al., Distribution and localization of caveolin-1 in sinusoidal cells in rat liver, Med. Electron Microsc. 36 (2003) 33–40.
[28] C. Fernández-Hernando, J. Yu, Y. Suárez, C. Rahner, A. Dávalos, M.A. Lasunción, et al., Genetic evidence supporting a critical role of endothelial caveolin-1 during the progression of atherosclerosis, Cell Metab. 10 (2009) 148–154.
[29] A. Warren, V.C. Cogger, I.M. Arias, R.S. McCuskey, D.G. Le Couteur, Liver sinusoidal endothelial fenestrations in caveolin-1 knockout mice, Microcirculation 17 (2010) 32–38.
[30] K.J. Bubb, A.B. Birgisdottir, O. Tang, T. Hansen, G.A. Figtree, Redox modification of caveolar proteins in the cardiovascular system-role in cellular signalling and disease, Free Radic. Biol. Med. 109 (2017) 61–74.
[31] F. Chen, S. Barman, Y. Yu, S. Haigh, Y. Wang, S.M. Black, et al., Caveolin-1 is a negative regulator of NADPH oxidase-derived reactive oxygen species, Free Radic. Biol. Med. 73 (2014) 201–213.
[32] C. Trimmer, F. Sotgia, D. Whitaker-Menezes, R.M. Balliet, G. Eaton, U.E. Martinez-Outschoorn, et al., Caveolin-1 and mitochondrial SOD2 (MnSOD) function as tumor suppressors in the stromal microenvironment: a new genetically tractable model for human cancer associated fibroblasts, Cancer Biol. Ther. 11 (2011) 383–394.
[33] R. Baudrand, N. Gupta, A.E. Garza, A. Vaidya, J.A. Leopold, P.N. Hopkins, et al., Caveolin 1 modulates aldosterone-mediated pathways of glucose and lipid homeostasis, J. Am. Heart Assoc. 5 (2016) e003845.
[34] T. Nakamura, M. Fukuda, K. Kataoka, H. Nako, Y. Tokutomi, Y.F. Dong, et al., Eplerenone potentiates protective effects of amlodipine against cardiovascular injury in salt-sensitive hypertensive rats, Hypertens. Res. 34 (2011) 817–824.
[35] T.K. Ha, N.G. Her, M.G. Lee, B.K. Ryu, J.H. Lee, J. Han, et al., Caveolin-1 increases aerobic glycolysis in colorectal cancers by stimulating HMGA1-mediated GLUT3 transcription, Cancer Res. 72 (2012) 4097–4109.
[36] L.D. DeLeve, Liver sinusoidal endothelial cells in hepatic fibrosis, Hepatology 61 (2015) 1740–1746.
[37] G. Xie, X. Wang, L. Wang, L. Wang, R.D. Atkinson, G.C. Kanel, et al., Role of differentiation of liver sinusoidal endothelial cells in progression and regression of hepatic fibrosis in rats, Gastroenterology 142 (2012) 918–927.
[38] N. Toda, S. Nakanishi, S. Tanabe, Aldosterone affects blood flow and vascular tone regulated by endothelium-derived NO: therapeutic implications, Br. J. Pharmacol. 168 (2013) 519–533.
[39] Daisuke Nagata, Masao Takahashi, Kuniko Sawai, Tetsuya Tagami, Takeshi Usui, Akira Shimatsu, et al., Molecular mechanism of the inhibitory effect of aldosterone on endothelial NO synthase activity, Hypertension 48 (2006) 165–171.
[40] Jamaira A. Victorio, Stefano P. Clerici, Roberto Palacios, María J. Alonso, Dalton V. Vassallo, Iris Z. Jaffe, et al., Spironolactone prevents endothelial nitric oxide synthase uncoupling and vascular dysfunction induced by β-adrenergic Overstimulation: role of perivascular adipose tissue, Hypertension 68 (2016) 726–735.
[41] S. Sarkar, V.I. Korolchuk, M. Renna, S. Imarisio, A. Fleming, A. Williams, et al., Complex inhibitory effects of nitric oxide on autophagy, Mol. Cell 43 (2011) 19–32.
[42] C. Cheng, D. Tempel, A. Oostlander, F. Helderman, F. Gijsen, J. Wentzel, et al., Rapamycin modulates the eNOS vs. shear stress relationship, Cardiovasc. Res. 78 (2008) 123–129.